CHEMISTRY OF MATERIALS
Article

Chem. Mater. **2009,** *21,* 5215–5221 5215
DOI:10.1021/cm902128r

Chloro-Alkoxide Route to Transition Metal Oxides. Synthesis of WO_3 Thin Films and Powders from a Tungsten Chloro-Methoxide

Mauro Epifani,*[,†] Teresa Andreu,[‡] Jordi Arbiol,[§,∥] Raül Díaz,[‡,#] Pietro Siciliano,[†] and Joan R. Morante[‡,⊥]

[†]*Consiglio Nazionale delle Ricerche - Istituto per la Microelettronica e Microsistemi* (*C.N.R.-I.M.M.*), *via Monteroni, I-73100 Lecce, Italy;*, [‡]*M2E-IN2UB-XaRMAE, Departament d'Electrònica, Universitat de Barcelona, C. Martí i Franquès 1, 08028 Barcelona, CAT, Spain,* [§]*MIND-IN2UB, Dept. Electronica, Universitat de Barcelona, Marti i Franques 1, 08028 barcelona, CAT, Spain,* [∥]*ICREA Research Professor at Institut de Ciència de Materials de Barcelona, CSIC, 08193 Bellaterra, CAT, Spain, and* [⊥]*Institut de Recerca en Energia de Catalunya* (*IREC*), *C/ Josep Pla 2, B3, E-08019 Barcelona, Spain.* [#]*Current Address: Electrochemical Processes Unit, IMDEA Energy, c/Tulipan, s/n, E-28933 Mostoles* (*Madrid*), *Spain.*

Received July 14, 2009. Revised Manuscript Received September 3, 2009

A tungsten chloromethoxide was prepared by the methanolysis of WCl_6. The resulting solutions were modified by addition of acetylacetone to improve their stability. The resulting deep blue solutions were studied by infrared and Raman spectroscopy. The structure of the solutions was characterized by polynuclear tungsten species containing W—O—W bonds. The solutions were used for preparing thin films, by spin-coating onto oxidized silicon substrates, and powders, by evaporation at reduced pressure. The as-dried thin films and powders were heat-treated at various temperatures up to 700 °C and characterized by infrared and Raman spectroscopy and X-ray diffraction. The investigations showed that the precursor structure follows a continuous evolution to the final WO_3 structure, by further condensation and thermally activated reorganization of the initial species. The final crystalline structure was a mixture of the most stable δ-triclinic and γ-monoclinic phases. The absence of W═O groups both in the solutions and the final materials and the weakness of the W—Cl bond explained the lower stability of the solutions, if compared to oxychloride precursors like $WOCl_4$. The structure and morphology of the films, characterized by scanning and transmission electron microscopy, was constituted by discrete spheroidal grains, elongated along the substrate surface. Chemoresistive gas sensing devices were prepared with the WO_3 powders heat-treated at 500 °C and tested for the detection of ammonia and nitrogen dioxide. The results indicated the capability of the sensors to detect the target gases over a broad range of concentrations, with a stable signal.

Introduction

The scientific and technological importance of transition metal oxides continuously requires the study and development of suitable synthesis approaches. The sol−gel process has provided a general and affordable approach for the preparation of metal oxides in various forms, with a continuous evolution of the materials typologies, the exploited precursors, and the underlying chemistry. In an effort to develop alternative precursors to metal alkoxides,[1] we have been investigating the synthesis of chloro-alkoxides from solvolyzable metal chlorides. The aim was to overcome some conventional disadvantages of metal alkoxides, like the high cost and moisture sensitivity. In previous works, the synthesis of SnO_2,[2] MoO_3,[3] and V_2O_5[4] thin films and powders was developed from chloro-propoxides or chloro-methoxides. In this work, we continue the investigation of the chloro-alkoxides family as convenient sol−gel precursors and present the synthesis of a tungsten chloromethoxide from the methanolysis of WCl_6 and its successful application to the synthesis of WO_3 thin films and powders. This investigation was suggested by the observation that the solvolysis of WCl_6 has been extensively exploited for the sol−gel processing of WO_3,[5] aside from the much less

*Corresponding author. E-mail: mauro.epifani@le.imm.cnr.it.

(1) (a) Bradley, D. C.; Mehrothra, R. C.; Gaur, D. P. *Metal Alkoxides*; Academic Press: London, U.K., 1978; (b) Turova, N. Y., Turevskaya, E. P., Kessler, V. G., Yanovskaya, M. I., Eds. *The chemistry of metal alkoxides*; Springer: Heidelberg, Germany, 2002.

(2) Epifani, M.; Alvisi, M.; Mirenghi, L; Leo, G.; Siciliano, P.; Vasanelli, L. *J. Am. Ceram. Soc.* **2001**, *84*, 48–54.

(3) Epifani, M.; Imperatori, P.; Mirenghi, L.; Schioppa, M.; Siciliano, P. *Chem. Mater.* **2004**, *16*, 5495–5501.

(4) Epifani, M.; Andreu, T.; Magana, C. R.; Arbiol, J.; Siciliano, P.; D'Arienzo, M.; Scotti, R.; Morazzoni, F.; Morante, J. R. *Chem. Mater.* **2009**, *21*, 1618–1626.

(5) (a) Shieh, J.; Feng, H. M.; Hon, M. H.; Juang, H. Y. *Sens. Actuators, B* **2002**, *86*, 75–80. (b) Cheng, W.; Baudrin, E.; Dunn, B.; Zink, J. *J. Mater. Chem.* **2001**, *11*, 92–97. (c) Nishide, T.; Sawada, Y.; Habu, T.; Senda, T. *Thermochim. Acta* **1996**, *278*, 91–97. (d) Bechinger, C.; Muffler, H.; Schäfle, C.; Sundberg, O.; Leiderer, P. *Thin Solid Films* **2000**, *366*, 135–138. (e) Zayim, E. O.; Liu, P.; Lee, S.-H.; Tracy, C. E.; Turner, J. A.; Pitts, J. R.; Deb, S. K. *Solid State Ionics* **2003**, *165*, 65–72. (f) Nishio, K.; Tsuchiya, T. *Sol. Energy Mater. Sol. Cells* **2001**, *68*, 279–293. (g) Nishide, T.; Mizukami, F. *Thin Solid Films* **2002**, *86*, 212–217. (h) Badilescu, S.; Ashrit, P. V. *Solid State Ionics* **2003**, *158*, 187–197. (i) Tong, M.; Dai, G.; Gao, D. *Mater. Chem. Phys.* **2001**, *69*, 176–179.

Published on Web 10/07/2009

frequent processing of more unstable and expensive alkoxides,[6] but a study of the precursor evolution has been seldom carried out. In fact, precursor investigations concern only alkoxides[7] and $WOCl_4$.[8] Tungsten alkoxo and chloroalkoxo complexes[9] were widely investigated in the past, but with focus on their synthesis and structure. The lack of a systematic study of the WO_3 synthesis from WCl_6-derived chloroalkoxides (only ref 8 contained some related results, to the best of our knowledge) stimulated us to investigate in detail such an approach, to add it to the family of the previously mentioned metal chloroalkoxides. The obtained tungsten chloromethoxide resulted in being less stable among the chloro-alkoxides investigated up to now, which was explained with the limited strength of the W—Cl bond and the absence of W═O bonds. Nevertheless, WO_3 thin films and powders could be easily prepared without any particular apparatus for controlling the environmental moisture, and the precursor stability was extended over more than one month. The final material could be successfully processed in the fabrication of gas-sensing devices, which proved to be reliable and stable over a broad concentration of NO_2 and NH_3 test gases.

Experimental Section

WCl_6, methanol, and cetyltrimethylammonium bromide (CTAB) (Sigma-Aldrich) were used as received. Silicon substrates (⟨100⟩ orientation) with a 5000 Å SiO_2 overlayer were provided by ST Microelectronics. For methanolysis of WCl_6, 10 mL of MeOH were slowly added to 1 g of WCl_6 in a glovebox (Braun, LabStar) with $H_2O < 1$ ppm. A yellowish solution was obtained, which slowly turned faintly yellow and finally deep blue. After a few days, the solution was again faint yellow and contained a very small amount of a tiny blue precipitate. This solution could not be easily processed, since exposure to the atmosphere made it rapidly opaque with the formation of a precipitate. Hence, WCl_6 was reacted with a solution of acetylacetone (acacH, with acacH: W molar ratio of 3) in 10 mL of MeOH. After a fast color change, from yellow to orange, a deep blue solution was finally obtained. The solution, kept in a closed vial, was stable for more than one month, after which a blue precipitate deposited on the walls and the bottom of the vial. No water was added to the solutions, since it resulted in fast precipitation. For preparing thin films, the solution was further diluted with 10 mL of methanol, to improve its stability. Moreover, 30 mg of CTAB were added to the thin film solutions, for improving the adhesion to the silicon substrates. One day after the CTAB addition, the solution was spin-coated at 2000 rpm onto the silicon substrates, after precleaning for 2 min in boiling isopropanol. The films were dried for 3 min at 80 °C in air and then heat-treated for 1 h at temperatures ranging from 100 to 500 °C in air atmosphere in a tubular furnace, with a heating rate of 300 °C/h. The films were very uniform and crack-free after the various heat-treatments. The thickness of a film heat-treated at 500 °C was about 50 nm, as measured with a profilometer (Tencor Instruments, Alpha-Step IQ). Powders were prepared from the solutions by evaporation in a rotary evaporator at a pressure decreased from 100 mbar to 40 mbar in 30 min and with the bath temperature raised from RT to 80 °C in 1 h. The resulting product was a deep blue, redispersible powder. The evaporation product was heat-treated at various temperatures similarly to the thin films, obtaining a bright yellow powder after heat-treating at temperatures higher than 300 °C.

The green line (λ = 514 nm) of a Jobin Yvon T64000 spectrometer with an INNOVA 300 Coherent Ar laser and a bidimensional CCD detector cooled with liquid nitrogen was used for Raman analysis of the solutions and powders.

Fourier transform infrared (FTIR) spectroscopic measurements were carried out on the solutions with a Bomem MB-120 FTIR spectrometer, in a range from 350 to 4000 cm^{-1}, with a maximum resolution of 1 cm^{-1}. The solution samples were prepared by placing a drop of the solution on a KBr pellet and then evaporating the solvent at room temperature. FTIR spectra on the powders were measured on pellets prepared by mixing the powders with KBr. The sample/KBr volume ratio was about 1:50.

X-ray diffraction (XRD) measurements were performed on a Panalytical diffractometer working with the Cu Kα radiation (λ = 1.5406 Å) using a Bragg−Brentano geometry. For thin film measurements, the sample was tilted by 2° to reduce the intensity of the silicon substrate.

The morphology of the thin films was observed with a JEOL JSM6500F FEG scanning electron microscope.

High-resolution transmission electron microscopy (HRTEM) observations of the thin films were carried out with a field emission gun microscope Jeol 2010F, working at 200 kV and with a point-to-point resolution of 0.19 nm.

The gas-sensing tests on devices prepared with the WO_3 powders heat-treated at 500 °C were carried out using a standard configuration for resistive sensor measurement, with Pt-interdigitated electrodes and a Pt-resistive-type heater printed onto an alumina substrate. Sensors were prepared by depositing a mixture of the WO_3 powder with 1,2-propanediol onto interdigitated electrodes and subsequently annealing at 400 °C for 1 h to burn the organic binder and to ensure sample adhesion to the alumina surface. The sensor devices were placed in a sealed chamber with a constant flux of 0.2 L/min of synthetic air into which the desired amount of test gases was mixed. The sensor response was defined as R_{air}/R_{gas} and R_{gas}/R_{air} for reducing and oxidizing gases. Here, R_{air} and R_{gas} indicate the sensor electrical resistance before and after exposure to the target gas, respectively. The gases tested in the present work were NH_3 and NO_2.

Results and Discussion

A. Preparation and Properties of the Starting Solutions. When WCl_6 was reacted with only methanol, a yellowish solution was slowly obtained, as described in the Experimental Section, and already reported by, for instance, Klejnot[9a] and Judenstein and Livage.[8] This solution could not be easily handled, since exposure to air

(6) (a) Unuma, H.; Tonooka, K.; Suzuki, Y.; Furusaki, T.; Kodaira, K.; Matsushita, T. *J. Mater. Sci. Lett.* **1986**, *5*, 1248–1250. (b) Takase, A.; Miyakawa, K. *Jpn. J. Appl. Phys.* **1991**, *30*, L1508–L1511.
(7) Yanovskaya, M. I.; Obvintseva, I. E.; Kessler, V. G.; Galyamov, B. Sh.; Kucheiko, S. I.; Shifrina, R. R.; Turova, N. Ya. *J. Non-Cryst. Solids* **1990**, *124*, 155–166.
(8) Judeinstein, P.; Livage, J. *J. Mater. Chem.* **1991**, *1*, 621–627.
(9) (a) Klejnot, O. J. *Inorg. Chem.* **1965**, *4*, 1668–1670. (b) Rillema, D. P; Reagan, W. J; Brubaker, C. H.Jr. *Inorg. Chem.* **1969**, *8*, 587–590. (c) Rillema, D. P; Brubaker, C. H.Jr. *Inorg. Chem.* **1969**, *8*, 1645–1649. (d) Reagan, W. J; Brubaker, C. H.Jr. *Inorg. Chem.* **1970**, *9*, 827–830. (e) Handy, L. B.; Sharp, K. G.; Brinckman, F. E. *Inorg. Chem.* **1972**, *11*, 523–531. (f) Chisholm, M. H. *J. Solid State Chem.* **1985**, *57*, 120–133. (g) Clegg, W.; Errington, R. J.; Kraxner, P.; Redshaw, C. *J. Chem. Soc., Dalton Trans.* **1992**, 1431–1438.

rapidly made it unstable, with the onset of turbidity. The final yellow color, suggesting the presence of W(VI) species, indicated the aerial reoxidation of the blue W(V) species, formed upon initial reduction by methanol:[9a]

$$WCl_6 + 2CH_3OH \rightarrow WCl_3(OCH_3)_2 + 2HCl + \frac{1}{2}Cl_2 \quad (1)$$

$$CH_3OH + Cl_2 \rightarrow HCHO + 2HCl$$

Hence, the solution processing was modified by the addition of acetylacetone, aimed to slow down the bridging and condensation of the W(VI) species. The solution prepared in this way was much more stable upon exposure to the atmosphere and retained its deep blue color. The acacH-modified solutions were stable for about one month, much less if compared to the chloro-alkoxides of other elements. For getting more insight about these phenomena, the chemical structure of the solutions was investigated. The structure of tungsten polynuclear species is generally exceedingly complex, so we tried to get general trends from the solution characterization. In Figure 1, the FTIR and Raman spectra measured on the solutions are reported. Since the solutions for thin films and powders had a different tungsten concentration (see Experimental Section), both of them were analyzed. The Raman curve for the powder precursor solution is not shown since it is identical to that for thin films. The IR solution curves display common features, with some bands more remarked in the thin film curve. In the latter a typical methanol band at 1030 cm^{-1} is observed, due to the larger amount of solvent after sample evaporation, and above all two bands at 1730 and 1630 cm^{-1}, the latter being very strong.

These bands are typical of the carbonyl stretching of the keto and enol form of acetylacetone, respectively.[10] The position of the enol band is not typical of chelate formation, since in that case it would be shifted to lower wavenumbers.[11] Complex formation through the keto form is known,[12] but the synthesis conditions were much different from our experimental procedures. We concluded that acetylacetone is only able to hinder the formation of extended W—O—W bonds, without forming stable chelate species. The presence of W—O—W oligomers is suggested by a broad IR band below 800 cm^{-1}, a region where metal−oxygen−metal modes are typically found. The condensation of the solution

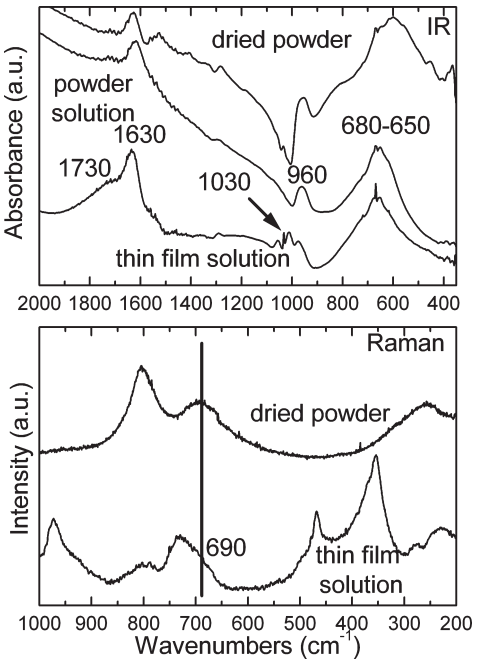

Figure 1. FTIR and Raman spectra measured on the solutions used for the thin film and powder preparation. For comparison, the spectra measured on the as-dried precursor powder are also shown. The vertical line in the Raman plot is only a guide to the eye.

oligomers results in more complex bands in the IR curve of the dried precursor powder. In the bottom panel of Figure 1, the Raman spectra measured on the same samples are reported. As in IR spectra, solution bands resembling those of the dried precursor were found, in particular at 690 cm^{-1} (shoulder) and at about 810 cm^{-1}. Again these bands were attributed to W—O—W modes. In the solution spectrum, these bands are still weak and not as resolved as in the dried sample, but they clearly indicate the presence of extended bonds. From these results it emerges that the tungsten chloroalkoxide has a remarkable polymerization tendency and that the addition of acetylacetone delays further polymerization to larger species. A first reason of the chloroalkoxide polymerization tendency was indicated by the XPS spectra measured on as-dried (80 °C, not shown) thin films. The data evidenced the absence of chlorine, which is an indication of the limited strength of the W—Cl bonds. Further insight about the precursor stability was obtained by the investigation of the structural evolution upon drying and heat treatments, reported in the next section.

B. Precursor Evolution upon Drying and Heat Treatment. Figure 2A shows the XRD patterns measured on the dried precursor heat-treated at increasing temperatures. Up to 300 °C, the patterns show only very broad reflections, indicating a mainly amorphous material. After heat-treating at 400 °C, diffraction peaks are clearly observed. The WO_3 structure is constituted by a three-dimensional network of corner-sharing octahedra. Network distortion with respect to the ReO_3 model structure, due both to tungsten displacement from the octahedron

(10) Colthup, N. B.; Daly, L. H.; Wiberley, S. E. *Introduction to Infrared and Raman Spectroscopy*, 3rd ed.; Academic Press: San Diego, CA, 1990.
(11) (a) Nakamoto, K. *Infrared and Raman Spectra of Inorganic and Coordination Compounds. Part B: Applications in Cooordination, Organometallic, and Bioinorganic Chemistry*, 5th ed.; Wiley: New York, 1997. (b) Thornton, D. A. *Coord. Chem. Rev.* **1990**, *104*, 173–249.
(12) (a) Nakamura, Y.; Kawaguchi, S. *Chem. Commun.* **1968**, 716. (b) Koda, S.; Ooi, S.; Kuroya, H.; Nakamura, Y.; Kawaguchi, S. *Chem. Commun.* **1971**, 280–281. (c) Koda, S.; Ooi, S.; Kuroya, H.; Isobe, K.; Nakamura, Y.; Kawaguchi, S. *Chem. Commun.* **1971**, 1321–1322. (d) Nakamura, Y.; Isobe, K.; Morita, H.; Yamazaki, S.; Kawaguchi, S. *Inorg. Chem.* **1972**, *11*, 1573–1578.

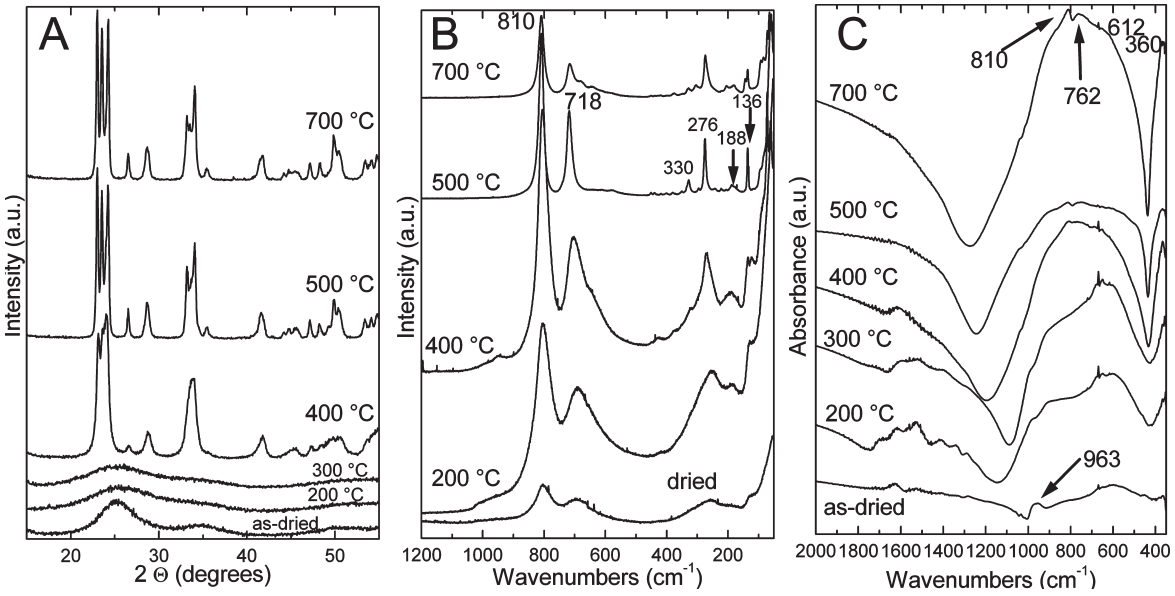

Figure 2. XRD patterns (A), Raman (B), and FTIR (C) spectra measured on the precursor powders heat-treated at the indicated temperatures.

center and tilting of the octahedra, gives rise to a complex system of phase transitions.[13]

Upon cooling, the γ monoclinic phase is generally reported as the stable one at 25 °C. This finding has been questioned, since there is some evidence that the δ triclinic phase is the most stable at room temperature. In any case, the XRD patterns of the two phases are hardly distinguished, and it is usual to find their coexistence at room temperature.[14] After heat-treatment at 400 °C, the pattern is in fact identified as belonging to the γ or δ phase.[15] The peaks are not completely resolved, indicating small size of the WO_3 crystallites. With increasing the heating temperature, the peaks are sharpened and resolved due to the particle size increase, but the pattern structure does not present obvious changes, even after heat treatment at 700 °C.

The Raman and IR data for powders are shown in panels B and C of Figure 2, respectively. In the Raman spectra, three regions between 900 and 600, 400 and 200, and below 200 cm^{-1} are clearly distinguished, which are due to stretching (ν O—W—O), deformation (δ O—W—O), and lattice modes of WO_3, respectively, as firmly established in early studies.[16] In the IR spectra the same characteristic modes are observed, despite being overlapped by the band broadening. In Figure 2B, with increasing the heating temperature a slight shift and remarked sharpening of the main bands is observed with increasing the heating temperature, and up to 400 °C the intense stretching bands (818 and 710 cm^{-1}) are distorted, in agreement with the evolution of the XRD patterns. Similar conclusions can be drawn from the evolution of the IR spectra in Figure 2C. The resemblance between the Raman and IR spectra of the dried precursor and those of the powders heat-treated at higher temperatures is not commonly observed in other systems. This result suggests the presence of highly cross-linked species already after the drying step. If we further recall the resemblance between the solution and dried precursor spectra in Figure 1, the picture that emerges is that of a continuous precursor evolution, from the solution to the final crystalline structure, just dictated by the enhanced cross-linking tendency of the starting chloroalkoxide.

Another important result is related to the possible reasons for the low solution stability with respect to other chloroalkoxides. A band at about 960 cm^{-1} is observed in Figure 2C in the dried precursor, which disappears completely after heat-treating at 400 °C. In general this band is typical of metal=O stretching mode in metal oxides,[17] but then it should be observed also in Raman spectra, while in Figure 2B it is missing. We then attributed it to the W(O−C) stretching, since the latter is known to occur in this region for metal alkoxides, concluding that no W=O bonds exist in solution. The absence of the W=O bond is important for explaining the low solution stability, together with the lability of the W—Cl bond. In the presence of a W=O bond, the condensation pathways between different oligomers in solution are reduced, delaying the formation of larger species.

(13) (a) Kehl, W. L.; Hay, R. G.; Wahl, D. *J. Appl. Phys.* **1952**, *23*, 212–215. (b) Loopstra, B. O.; Boldrini, P. *Acta Crystallogr.* **1966**, *21*, 158–162. (c) Loopstra, B. O.; Rietveld, H. M. *Acta Cryst. B* **1969**, *25*, 1420–1421. (d) Salje, E. *Ferroelectrics* **1976**, *12*, 215–217. (e) Salje, E. *Acta Cryst. B* **1977**, *33*, 574–577. (f) Diehl, R.; Brandt, G.; Salje, E. *Acta Cryst. B* **1978**, *34*, 1105–1111. (g) Woodward, P. M.; Sleight, A. W.; Vogt, T. *J. Phys. Chem. Solids* **1995**, *56*, 1305–1315. (h) Woodward, P. M.; Sleight, A. W.; Vogt, T. *J. Solid State Chem.* **1997**, *131*, 9–17. (i) Salje, E. K. H.; Rehmann, S.; Pobell, F.; Morris, D.; Knight, K. S.; Herrmannsdorfer, T.; Dove, T. M. *J. Phys.: Condens. Matter* **1997**, *9*, 6563–6577.

(14) (a) Cazzanelli, E.; Vinegoni, C.; Mariotto, C.; Kuzmin, A.; Purans *J. Solid State Chem.* **1999**, *143*, 24–32. (b) Souza-Filho, A. G.; Freire, V. N.; Sasaki, J. M.; Mendes Filho, J.; Juliao, J. F.; Gomes, U. U. *J. Raman Spectrosc.* **2000**, *31*, 451–454.

(15) JCPDS cards: 83-0947 (triclinic) and 43-1035 (monoclinic).

(16) (a) Salje, E. *Acta Crystallogr., Sect. A* **1975**, *31*, 360–363. (b) Daniel, M. F.; Desbat, B.; Lassegues, J. C.; Gerand, B.; Figlarz, M. *J. Solid State Chem.* **1987**, *67*, 235–247.

(17) Nakamoto, K. *Infrared and Raman Spectra of Inorganic and Coordination Compounds. Part B: Applications in Cooordination, Organometallic, and Bioinorganic Chemistry*, 5th ed.; Wiley: New York, 1997; p 168.

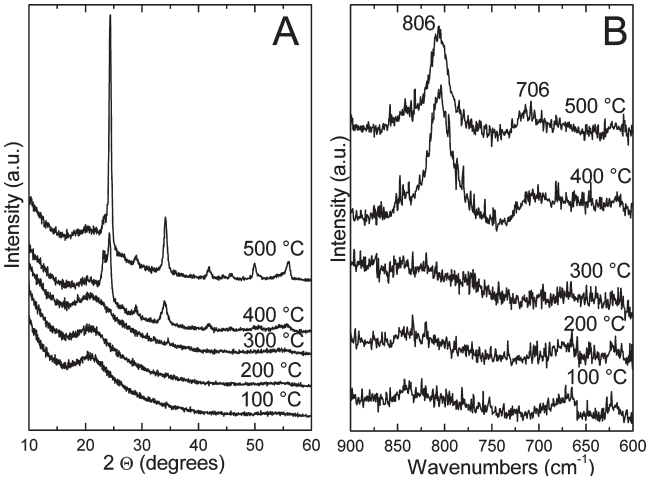

Figure 3. XRD patterns (A) and Raman spectra (B) measured on thin films heat-treated at the indicated temperatures.

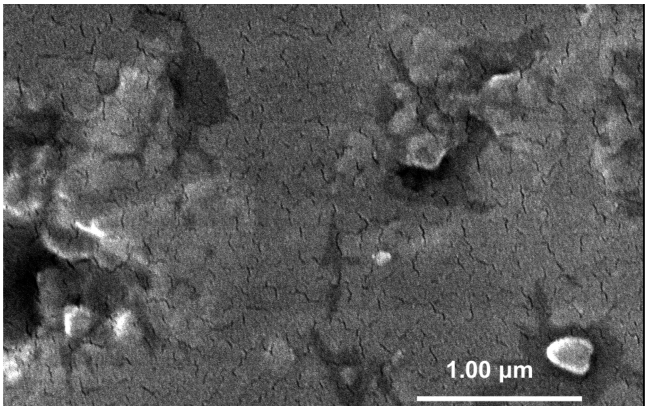

Figure 4. FE-SEM image of a WO_3 thin film heat-treated at 500 °C.

The evolution of the W(V) species was monitored by electron paramagnetic resonance (EPR) spectroscopy. The solution spectrum shows a single signal, indicating weak interaction between the W(V) centers, while the signal becomes much more complex in the solid samples. The W(V) signal is strongly reduced after the heat-treatment at 500 °C, in agreement with the formation of the W(VI) in the final oxide. These results did not show obvious deviations from the expected behavior, so they are shown in the Supporting Information.

The XRD patterns and Raman spectra of thin films heat-treated at various temperatures are reported in Figure 3A, B, respectively. The comparison with the powder results shows that the precursor thermal evolution for thin films follows similar pathways. In Figure 3A, WO_3 crystallization takes place after heat-treatment at 400 °C, just like in powder materials, and this result is closely followed by the Raman spectra in Figure 3B. The resemblance between the powder and thin film results indicates a very similar precursor evolution for both materials typologies.

C. Morphology and Structure of Thin Films. The morphology and structure of only the thin films was studied due to powder aggregation after the heat treatment, preventing a clear observation of the crystallites, which anyway have a large size, as deduced from the XRD patterns in Figure 2A. In Figure 4 the surface morphology of a thin film heat-treated at 500 °C is shown. Despite the films being highly uniform by the naked eye, the situation is different in FE-SEM observations.

At high magnification, the film shows very small microcracks. Moreover, some voids are occasionally observed, as shown in the sample image of Figure 4. The reason for the surface morphology is suggested by the cross-sectional TEM observations, whose results are reported in Figure 5. The WO_3 layer presents an inhomogeneous thickness ranging from 15 to 50 nm. The general view TEM image shows a structure constituted by attached spheroidal grains, which tend to be elongated along the substrate surface. Other images are shown in the Supporting Information (Figures S1 and S2). The low hydrolytic stability of our precursor results in dense structures during the fast film formation in the spin-coating stage. These structures are less amenable to interpenetrating and forming a polymeric, extended layer. The resulting film is then less able to resist to the mechanical stress originated in the drying and heat-treatment step, which explains the microcracks and the thickness irregularities observed over a long length range. On the other hand, Judeinstein and Livage[8] reported a longer stability of the solutions and uniform and thicker films than ours, similarly to Ozer[18] who also used $WOCl_4$ as initial precursor. It then seems that the presence of the W=O bond and the consequent control of the hydrolysis rate during the film deposition may improve the structural properties of the final materials. The remaining images in Figure 5 complete the structural characterization, showing a high-resolution image and the related power spectrum. The presence of WO_3 crystallites is confirmed, but even in this case it is not easy to distinguish between the monoclinic and triclinic phase. Nevertheless in the simulations of the power spectra the best fitting was obtained for triclinic WO_3 structure.

D. Sensing Properties of WO_3 Powders. As a part of a program for the development of materials for gas-sensing applications, the gas-sensing properties of the WO_3 powders were evaluated. WO_3 has been particularly investigated for detecting NO_2[19] and NH_3,[20] but also H_2S and CO[21] were included in the target gases. Chemoresistive gas-sensors were prepared by using the powders heat-treated at 500 °C, as described in the Experimental Section. Ammonia and nitrogen dioxide were tested as sample analytes for reducing and oxidizing gases, respectively. In the

(18) Ozer, N. *Thin Solid Films* **1997**, *304*, 310–314.
(19) (a) Akiyama, M.; Tamaki, J.; Miura, N.; Yamazoe, N. *Chem. Lett.* **1991**, 1611–1614. (b) Akiyama, M.; Zhang, Z.; Tamaki, J.; Miura, N.; Yamazoe, N. *Sens. Actuators, B* **1993**, *14*, 619–620. (c) Tamaki, J.; Hashishin, T.; Uno, Y.; Dao, D. V.; Sugiyama, S. *Sens. Actuators, B* **2008**, *132*, 234–238. (d) Kida, T.; Nishiyama, A.; Yuasa, M.; Shimanoe, K.; Yamazoe, N. *Sens. Actuators, B* **2009**, *135*, 568–574.
(20) (a) Jimenez, I.; Centeno, M. A.; Scotti, R.; Morazzoni, F.; Cornet, A.; Morante, J. R. *J. Electrochem. Soc.* **2003**, *150*, H72–H80. (b) Jimenez, I.; Centeno, M. A.; Scotti, R.; Morazzoni, F.; Arbiol, J.; Cornet, A.; Morante, J. R. *J. Mater. Chem.* **2004**, *14*, 2412–2420. (c) Zhao, Y. M.; Zhu, Y. Q. *Sens. Actuators, B* **2009**, *137*, 27–31.
(21) (a) Jimenez, I.; Arbiol, J.; Dezanneau, G.; Cornet, A.; Morante, J. R. *Sens. Actuators, B* **2003**, *93*, 475–485. (b) Azad, A.-M.; Hammoud, M. *Sens. Actuators, B* **2006**, *119*, 384–391. (c) Ruiz, A. M.; Illa, X.; Diaz, R.; Romano-Rodriguez, A.; Morante, J. R. *Sens. Actuators, B* **2006**, *118*, 318–322.

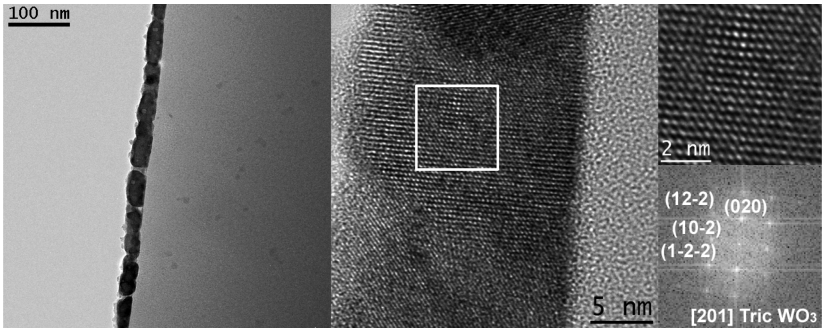

Figure 5. From left to right: TEM general view image of a WO_3 thin film heat-treated at 500 °C, high-resolution magnification of a region within the same film, detail of the marked high-resolution area, and related power spectrum.

Supporting Information the stabilization data of the devices are reported (Figure S3), showing a very stable signal over a broad temperature range, with a base electrical resistance value ranging around 10^5 Ω−1 MΩ.

In Figure 6 the dynamic response curves to NH_3 and NO_2 are shown, for operating temperatures ranging from 200 to 350 °C. In both cases, a slight drift of the baseline is observed at 200 °C, when switching from a gas concentration to the following.

For higher operating temperatures, the signal becomes very stable, and a full and fast recovery is obtained after removing the analyte from the test chamber. As expected from the interaction of reducing and oxidizing gases with a n-type semiconductor, a resistance drop is observed upon exposure to ammonia and the reverse for NO_2. From the dynamic curves, an appreciable variation of the electrical signal occurs upon injection of each gas concentration. For evaluating in detail the capability of the sensor to detect the test gases, the response was calculated for each operating temperature. The response of the sensor is defined as R_0/R_{GAS} and R_{GAS}/R_0 for reducing and oxidizing gases, respectively, where R_0 and R_{GAS} are the saturation electrical resistances in pure air and in the test gas, respectively.

In Figure 7 the resulting calibration curves for NH_3 testing are shown. The linear fit of the experimental points in log−log scale shows that the response follows the typical power laws for semiconducting chemoresistive sensors. For each concentration, the response first increases sharply from 200 to 225 to 250 °C. Further increase of the operating temperature does not further affect the response up to 300 °C, and then the latter decreases. These last observations are summarized for the 100 ppm concentration in the inset of Figure 7. A temperature of 250 °C then appears as the best operating condition, in terms of response magnitude and simultaneous reduction of the power consumption. Moreover, it improves the sensor stability if compared to higher operating temperatures. A satisfactory response is obtained for all the concentrations from 50 to 500 ppm, indicating the suitability of the sensor in the detection of ammonia in concentrations of practical interest. In Figure 8, the calibration for NO_2 sensing is shown. As expected from the generally accepted sensing mechanism for NO_2, based on gas adsorption onto the semiconductor

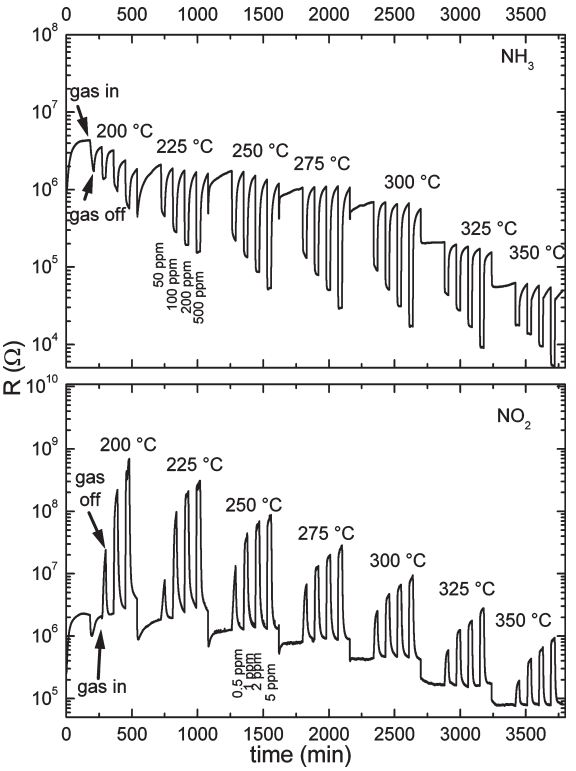

Figure 6. Dynamic response curves of sensors prepared with WO_3 powders heat-treated at 500 °C. In the upper panel the results are reported for ammonia, while in the bottom panel the data are for nitrogen dioxide.

surface, the response steadily decreases when increasing the operating temperature above 250 °C, which once again appears as the best operating condition. It is to be noted that the experimental points are fitted by a line only above 0.5 ppm concentration.

Moreover, for 0.5 ppm the response difference between 250 °C and higher operating temperatures is not as remarkable as for the higher concentrations. This observation suggests the presence of more complex sensing mechanisms at lower NO_2 concentrations. Even for NO_2 the responses, ranging over 2 orders of magnitude for 5 ppm concentration, indicate the capability of the sensor of reliably detecting the gas over a broad concentration range.

In the case of ammonia sensing, the chloroalkoxide route is convenient in avoiding the sensor instabilities previously observed with WO_3 prepared from H_2WO_4[20] and provides responses comparable, at a much lower

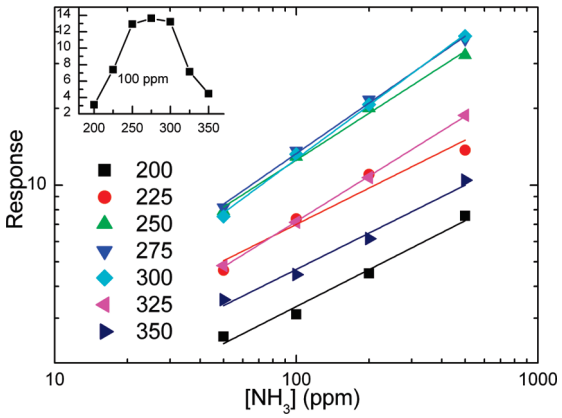

Figure 7. Calibration curves for NH_3 sensing at the indicated operating temperatures. The inset shows in detail the temperature dependence of the response to 100 ppm of NH_3.

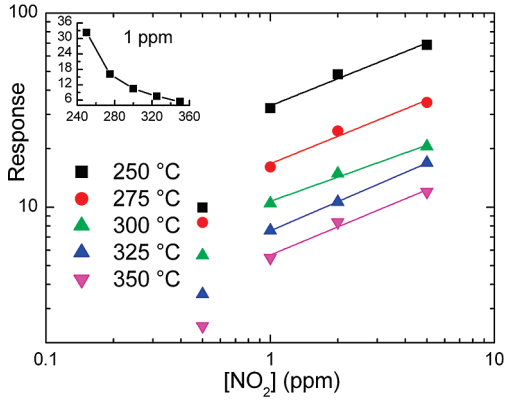

Figure 8. Calibration curves for NO_2 sensing at the indicated operating temperatures. The inset shows in detail the temperature dependence of the response to 1 ppm of NO_2.

operating temperature, to those obtained with WO_3 prepared with ammonium paratungstate.[22] WO_3 for NO_2 detection has been prepared by processing phosphotungstic acid (mesoporous structures),[23] sodium tungstate,[24] tungsten chloroalkoxide[25] and in the form of nanorods (assembled in microspheres), by hydrothermal processing of ammonium tungstate and oxalic acid.[26] The responses obtained with our sensors are comparable or even better with respect to such investigations and, if coupled with the easy material preparation, even in multigram scale, and the stable and recoverable signal, they make the chloroalkoxide route a convenient approach to these kinds of sensors. As expected, further NO_2 sensing breakthrough is only obtained with nanosized WO_3 based devices.[27]

Conclusions

The methanolysis of WCl_6, in the presence of acetylacetone, results in tungsten chloroalkoxo oligomers solutions with an improved stability with respect to the absence of acetylacetone but with enhanced precipitation with respect to other metal chloroalkoxides, due to the limited strength of the W—Cl bond and the absence of W=O groups. The solutions can be conveniently used for the deposition of WO_3 thin films and the preparation of WO_3 powders without a stringent control of the environmental moisture. A continuous evolution of the initial oligomers, through extended condensation, is responsible for the formation of the final crystalline product, a mixture of the monoclinic and triclinic crystallographic phases. The WO_3 powders were used for fabricating chemoresistive gas sensors, showing stable and reliable response over a broad concentration range of NH_3 and NO_2.

After adding the study of tungsten chloroalkoxide to our previous investigations, some considerations can be drawn concerning the common applicability field of such precursors. First of all, we observed that the chloro-alkoxide solutions display a remarkable time stability with respect to the corresponding alkoxide; moreover, they can be easily processed even in the presence of moisture to provide thin films and powders; finally, the residual chlorine is eliminated during the heat treatments or even after the spin-coating step, so the purity of the final material is not affected. These precursors display further applicability in the synthesis of nanomaterials, where we have successfully used them for the preparation of SnO_2 and TiO_2 nanocrystals.[28] The main disadvantages concern the limited functionality imparted by the residual chlorine (which, on the other hand, provides the advantage of stability): three-dimensional networking in the long range is expected to be more difficult with these precursors; moreover, elements such as V and W are characterized by a complex inorganic polymerization behavior, which makes difficult the use of their chloroalkoxides as nanomaterials precursors.

Acknowledgment. The authors are grateful for the use of the TEM-MAT, XRD, Raman, and FTIR units and the platform of polymorphism and calorimetry for TGA-DSC measurements of the Serveis Cientificotècnics of the Universitat de Barcelona.

Supporting Information Available: TEM and stabilization electrical data (PDF). This material is available free of charge via the Internet at http://pubs.acs.org.

(22) Wang, X.; Miura, N.; Yamazoe, N. *Sens. Actuators, B* **2000**, *66*, 74–76.
(23) Rossinyol, E.; Prim, A.; Pellicer, E.; Rodriguez, J.; Peiró, F.; Cornet, A.; Morante, J. R.; Thian, B.; Bo, T.; Zhao, D. *Sens. Actuators, B* **2007**, *126*, 18–23.
(24) Choi, Y.-G.; Sakai, G.; Shimanoe, K.; Miura, N.; Yamazoe, N. *Sens. Actuators, B* **2003**, *95*, 258–265.
(25) Blo, M.; Carotta, M. C.; Galliera, S.; Gherardi, S.; Giberti, A.; Guidi, V.; Malagù, C.; Martinelli, G.; Sacerdoti, M.; Vendemiati, B.; Zanni, A. *Sens. Actuators, B* **2004**, *103*, 213–218.
(26) Liu, Z.; Miyauchi, M.; Yamazaki, T.; Shen, Y. *Sens. Actuators, B* **2009**, *140*, 514–519.
(27) (a) Kida, T.; Nishiyama, A.; Yuasa, M.; Shimanoe, K.; Yamazoe, N. *Sens. Actuators, B* **2009**, *135*, 568–574. (b) Pokhrel, S.; Simion, C. E.; Teodorescu, V. S.; Barsan, N.; Weimar, U. *Adv. Mater*. **2009**, *19*, 1767–1774.
(28) (a) Epifani, M.; Díaz, R.; Arbiol, J.; Comini, E.; Sergent, N.; Pagnier, T.; Siciliano, P.; Faglia, G.; Morante, J. R. *Adv. Funct. Mater*. **2006**, *16*, 1488–1498. (b) Epifani, M.; Arbiol, J.; Andreu, T.; Morante, J. R. *Eur. J. Inorg. Chem*. **2008**, 859–862.